Eleventh International Conference on CFD in the Minerals and Process Industries
CSIRO, Melbourne, Australia
7-9 December 2015

DEM PARAMETER IDENTIFICATION BY MEANS OF ARTIFICIAL NEURAL NETWORK FOR IRON ORE SINTERING

Luca BENVENUTI[1*], Christoph KLOSS[2], Stefan PIRKER[1],

[1] JKU Department of Particulate Flow Modelling, 4040 Linz, Austria

[2] DCS Computing, 4040 Linz, Austria

*Corresponding author, E-mail address: luca.benvenuti@jku.at

ABSTRACT

Particle-particle contact laws and particles size distributions determine the macroscopic simulation results in Discrete Element Method (*DEM*). Commonly, contact laws depend on semi-empirical parameters which are difficult to obtain by direct microscopic measurements. Consequently, macroscopic experiments are performed, and the relationship between their results and microscopic DEM simulation is investigated.

We present a method for the identification of *DEM* simulation parameters though macroscopic experiments and dedicated artificial neural networks. First, a feed-forward artificial neural network is trained by backward propagation reinforcement thanks to the macroscopic results of a series of *DEM* simulations, each with a different set of particle-based simulation parameters and individual particle distributions. We subsequently utilize this artificial neural network to forecast the macroscopic ensemble behaviour in relation to additional sets of particle-based simulation parameters and particle distributions. By this method, a comprehensive database was established, relating particle-based simulation parameters to macroscopic ensemble output. If compared to an experiment of a specific granular material, this database identifies valid sets of *DEM* parameters which lead to the same macroscopic results as observed in the experiments. Finally, we applied this method of *DEM* parameter identification to an industrial scale process of iron ore sintering.

NOMENCLATURE

Greek Symbols

Δt	time step, [s]
μ	coefficient of friction, [-]
ν	Poisson ratio, [-]
ρ	mass density, [kg/m^3]
σ	stress, [Pa]
τ	shear stress, [Pa]

Latin Symbols

AOR	angle of repose, [-]
COR	coefficient of restitution, [-]
E	Young's modulus, [N/m^2]
R	radius of the particle, [m]

Sub/superscripts

b	bulk
n	normal
p	particle
psh	pre-shear
u	velocity
s	sliding
sh	shear
t	tangential

INTRODUCTION

Particles in various forms - ranging from raw materials to food grains and pharmaceutical powders - play a major role in a variety of industries. Discrete Element Methods (*DEMs*) are widely used to simulate particle behaviour in these granular processes (Cleary, Sawley 2002).

In their original formulation of *DEM*, Cundall and Strack (1979) allowed two particles to slightly overlap upon contact, and consequently they proposed repulsive forces in relation to this overlap distance. Their fundamental modelling concept has since been widely accepted in the literature and their soft-sphere contact law has been developed further by numerous researchers (Vu-Quoc, Zhang 1999, Di Renzo, Di Maio 2004). With increasing computational resources, *DEM* simulation have become very popular giving rise to the development of commercial (e.g., *PFC3D*, used by Wensrich and Katterfeld (2012)) and open-source software (e.g., *LIGGGHTS*, (Kloss, Goniva et al. 2012, Aigner, Schneiderbauer et al. 2013)). Soft-sphere *DEM* simulations of thousands of particles have been proven to faithfully model particle bulk behaviour (Kloss, Goniva et al. 2012).

In these macroscopic *DEM* simulations, the contact law kernel between a pair of particles determines the global bulk behaviour of the granular material (Ai, Chen et al. 2011). As a consequence, defining a correct contact law is of crucial importance for the predictive capability of *DEM* simulations. Since *DEM* contact laws are based on a set of semi-empirical parameters, correct contact law parameters must be defined for a given granular material or *DEM* simulations will fail (Combarros, Feise et al. 2014). Identifying *DEM* contact law parameters is not a trivial task. Due to the huge number of particles in a granular material, it may be impractical to identify valid parameter sets by performing bilateral particle collision experiments. Furthermore, some contact law parameters such as the coefficient of rolling friction are purely empirical and cannot be determined by direct particle-to-particle measurements (Wensrich, Katterfeld 2012). Therefore, *DEM* contact law parameters are commonly determined by comparing the macroscopic outcome of large-scale *DEM* simulations with bulk experiments (Alenzi, Marinack et al. 2013). If *DEM* simulation results disagree with bulk measurements, the set of contact law parameters must be adjusted until reasonable agreement is achieved.

However, this purely forward methodology of parameter identification is limited by the multi-dimensionality of the parameter space and the associated computational costs of the required *DEM* test simulations. Moreover, one parameter set which is valid for one bulk behaviour (e.g., angle of repose) might fail for another (e.g., shear tester).

Clearly, there is a need for an efficient method for identifying *DEM* contact law parameters. In our study, we harnessed Artificial Neural Networks (*ANNs*) in order to reduce the number of *DEM* test simulations required. *ANNs* have proven to be a versatile tool in analysing complex, non-linear systems of multi-dimensional input streams (Vaferi, Samimi et al. 2014). In our case, we fed an *ANN* with *DEM* contact law parameters as input and compared the output with the bulk behaviour predicted by a corresponding *DEM* simulation. The difference between *ANN* prediction and *DEM* prediction is used to train our specific *ANN* with a backward-propagation algorithm (described further below). After a training phase comprising a limited number of *DEM* test simulations, the *ANN* can then be used as a stand-alone prediction tool for the bulk behaviour of a granular material in relation to *DEM* contact law parameters.

In this study, we applied this parameter identification method to two different granular bulk behaviours, namely the angle of repose (*AoR*) test and the Schulze shear cell (*SSC*) test. In both cases, we first trained a specific *ANN* using a number of *DEM* test simulations before we identified valid sets of *DEM* contact law parameters by comparing the stand-alone *ANN* predictions with corresponding bulk experiments. The *ANN* is validated thanks to standard statistical methods. For both cases we obtained valid sets of contact law parameters, which we then compared to formulate a reliable contact law for a given granular material. We further show that these data can be used to model an industrial scale process of iron ore sintering.

In the next section we define some prerequisites including *DEM* contact law definitions, a general description of the *ANN* functionality, and the proposed method of *DEM* contact law parameter identification. We then describe how it is applied to characterize the *DEM* contact law parameters of sinter fines.

DEM PARAMETER IDENTIFICATION

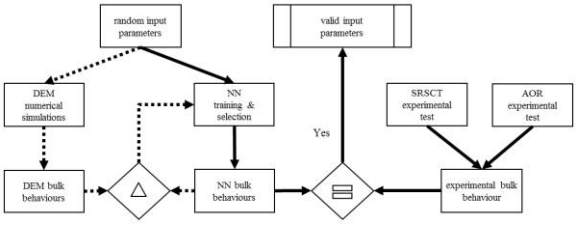

Figure 1: Method.

As can be seen in Figure 1, in the training phase (dashed lines) *DEM* simulations are performed with random initial input parameters. The behaviours obtained are used to train the Artificial Neural Networks (*ANNs*) in a loop that continues until the difference between the outputs of each *ANN* and its simulations is below the limit (Δ). In the parameters identification phase (solid lines) we identify valid input parameters by comparing (=) *ANNs* and experimental behaviours.

Discrete element method

Mean R (mm)	Std. dev R (mm)	Young's modulus (MPa)	Poisson's ratio (-)	Δt (s)
0.732	0.410	10.0	0.400	10^{-6}

Table 1: DEM fixed input values.

We decided to utilize a single contact law for all the simulations performed (Benvenuti, Kloss et al.). The *DEM* parameters for the Young's modulus (E) and the Poisson's coefficient (ν) were taken from the literature (Tsafnat, Amanat et al. 2011); however we reduced the former to increase the time step (Δt), following the recommendations of Ai, Chen et al. (2011). The time step was between 1.29% and 1.53% of the Rayleigh time, which also depends on the particle density (ρ_p). Furthermore, we locked the size distribution, which was obtained by experimental sieving, see Table 1. In the contact law we used, the tangential component of the contact force between two generic particles (F_t) is truncated to fulfil:

$$F_t \leq \mu_s \cdot F_n \tag{1}$$

where F_n is the normal component and μ_s is the coefficient of sliding friction, one of the particle-based *DEM* parameter we investigated, another being the coefficient of rolling friction (μ_r). For coarse non-spherical particles, this is a critical parameter and describes inter-particle friction in medium to dense granular flow simulations. It is proportional to the torque counteracting the rotation of the particle. The μ_r parameter enters the equations according to the elasto-rolling resistance model presented by Ai, Chen et al. (2011) and Wensrich and Katterfeld (2012). The model is called *EPSD2* in *LIGGGHTS* and is appropriate for both one-way and cyclical rolling cases. The maximum magnitude of rolling resistance torque:

$$T_{r\max} = \mu_r \cdot R_r \cdot \left|\widetilde{F_n}\right| \tag{2}$$

where R_r is the equivalent radius and F_n the normal force. The last two particle-based *DEM* parameters we investigated were ρ_p and the coefficient of restitution (*COR*) as defined by Ai, Chen et al. (2011). These coefficients, *COR*, μ_s, μ_r, ρ_p and *dCylDp* (the cylinder dimension, proportional to the mean particle diameter), as indicated in Table 2, were constant in each simulation, but their combination differed between simulations. Further, *dCylDp* was used to evaluate the wall effect, but only 10% of the simulations had a *dCylDp* larger than 20 (Benvenuti, Kloss et al.). The normal stress σ_n and its percentage during the incipient flow condition $\tau_{\%}$ varied to replicate twelve shear-cell load conditions. The complete description of the shear-cell and the *AoR* simulations can be found in Benvenuti, Kloss et al. and Benvenuti, Aigner et al. (2014). A Matlab script allowed us to extract from the simulation output the numerical values representative of bulk behaviour (hereafter called *bulk values*) for each DEM simulation parameter combination, which consists of bulk density (ρ_b), coefficient of internal friction in the pre-shear phase (μ_{psh}), coefficient of internal friction in the shear phase (μ_{sh}), and angle of repose (*AoR*). During the shear cell test the first bulk value (ρ_b) was provided directly. First, the σ_n was kept constant while the coefficient of internal friction (μ_{ie}) initially increased and then reached a plateau. The second bulk value (μ_{psh}) was

calculated as the average of the μ_{ie} in this plateau. The σ_n was then automatically reduced, e.g. to 80% of its initial value. Subsequently, a second plateau developed. We obtained the third value (μ_{sh}) as the average of μ_{ie} in this second plateau.
In the *AoR* tests the average of the repose angles provided us with the fourth bulk value, allowing us to define the numerical bulk behaviour.

μ_s (-)	μ_r (-)	COR (-)	ρ_p (kg/m^3)	DCylDp (-)
0.4 / 0.6 / 0.8	0.4 / 0.6 / 0.8	0.5 / 0.7 / 0.9	2500 / 3000 / 3500	20 / 36 / 38 / 40

Table 2: DEM variable input values for training the Artificial Neural Networks.

Artificial Neural Networks

	μ_s (-)	μ_r (mm)	COR (-)	ρ_p (kg/m^3)
Range	[0.1…1.0]	[0.1… 1.0]	[0.5… 0.9]	[2500… 3500]
No. of values	100	100	25	25

Table 3: DEM random input values. Within each range the indicated number of random values was chosen according to a standard uniform distribution.

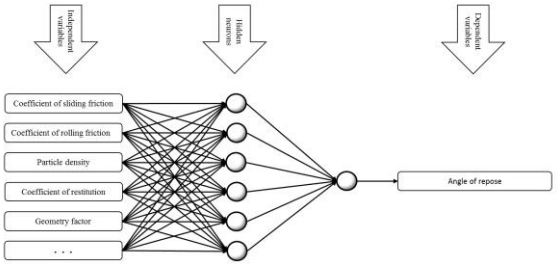

Figure 2: Scheme of how the Multilayer Perceptron *ANN* (*MLPNN*) derives one bulk-behaviour-dependent variable from the mutually independent simulation variables.

We first defined the typology of Artificial Neural Networks (*ANNs*) we used and the input we fed them (Benvenuti, Kloss et al.). Our *ANNs* have three different layers: the input layer has a number of neurons equal to the number of different inputs of the network, see **Figure 2**. The hidden (or central) layer's number of neurons was to be investigated. The output layer contains one neuron for the output. The transfer functions for the neurons of the central layer are the tangential sigmoid. Thus, we were able to use the *DEM* parameter combinations and their corresponding bulk values to train the *ANNs*. Especially, we divided the samples in three pools: the first, with 70% of the samples, as *training set*, the second, with 15% of the samples, as *generalization set*, for early stopping, and the third, as *test set*, as suggested by Haykin (2009). The assignment of each sample to each pool was random. We started with all the *DEM* parameter combinations and their corresponding numerical μ_{psh} from the *training set* to create 36 *ANNs* that differed in their numbers of neurons in the hidden layer (between five to forty neurons). The *generalization set* was used to speed the training. We then determined the coefficient of determination (R^2), between the *bulk-macro* behaviours in the output of the *ANN* and the *test set* simulations, which were not correlated with the remaining 70% used for the training. Thus, we could select for μ_{psh} the *ANN* with the maximum R^2, again as suggested by Vaferi, Samimi et al. (2014), and we noted its number of neurons. We then checked R^2, root mean squared error, mean absolute error, mean squared error of this *ANN* against a Bayesian linear regression and a Gaussian nonlinear regression to estimate the validity of the regression. Both were trained with the same *training set* as the *ANNs*. The check was performed for each method by comparing the *DEM bulk values* of the *test set* against the bulk values predicted by each method from the corresponding DEM input values of the *test set*.
We repeated the same *ANN* creation steps for μ_{sh}, ρ_b and *AoR*, obtaining one trained *ANN* for each bulk value. Since μ_{psh}, μ_{sh} and ρ_b belonged to the shear-cell simulations, their *ANNs* were handled together: we had one cluster with three *ANNs* for the shear cell and one with only one *ANN* for the *AoR*. We could then proceed in identifying valid input parameters. Oberkampf and Roy (2010) suggested using a Design of Experiments (*DoE*) method to determine the parameter combinations to be simulated. They stated that this approach allows optimization of computation time with an acceptable loss of precision. The speed of the trained *ANNs* enabled us to follow a different approach to maximizing the precision of the characterization. We created random values in the range and numbers defined in **Table 3** according to a standard uniform distribution. The total number of combinations of these random values was 6,250,000. These combinations were then fed to and processed by the selected *ANNs* and thus three bulk values for the shear cell and one for the *AoR* were obtained.

Macroscopic Experiments and Parameter Identification

The experimental characterization was performed as described in Benvenuti, Kloss et al. We obtained for each of the twelve load conditions of the *SSC* three bulk values (μ_{psh}, μ_{sh} and ρ_b). The fourth bulk value was the result of two angle of repose (*AoR*) tests that recreated the repose angle observed in a pile of the real material. Subsequently, we compared the *ANN* and experimental bulk behaviours for the twelve shear-cell load conditions. If in a DEM-parameter combination all the three bulk values differed by less than 5% from those of the corresponding experiments, i.e.:

$$\begin{cases} if & \left|1-\dfrac{\mu_{psh,num}}{\mu_{psh,\exp}}\right|<5\% \\ and\ if & \left|1-\dfrac{\mu_{sh,num}}{\mu_{sh,\exp}}\right|<5\% \\ and\ if & \left|1-\dfrac{\rho_{p,num}}{\rho_{p,\exp}}\right|<5\% \end{cases} \quad (3)$$

the combination was marked. The marked combinations were processed by the *AoR ANN*, and then compared with the experiment. We considered those valid those that differed by less than 5% also in this comparison:

$$if \left|1-\frac{AoR_{num}}{AoR_{\exp}}\right|<5\% \quad (4)$$

Application

The method previously explained allowed to collect data regarding the contact law. We took the average value for each of the *DEM* parameter and we used them in an industrial scale *DEM* simulation, with the same software, of an iron ore sintering process. Especially, we examined the behaviour of these particles in a sinter chute cooler. The particles moved from the top of a specifically designed chute and were collected by moving boxes at the bottom. These boxes were holed at the base, allowing cool air to lower the temperature of the sinter. It was critical to ascertain if the larger particles segregated, by moving to the bottom of the boxes, while the smaller to the top, allowing a more effective distribution of the cool air. The simulation was performed with a maximum of 500,000 particles.

RESULTS AND DISCUSSION

DEM simulations

For sinter fine, 546 shear cell and 81 static *AoR* simulations were run with the parameter combinations described in Table 2. The computational time amounted to 1 hour with 32 AMD cores for a benchmark shear-cell simulation and to 9 hours for a benchmark *AoR* simulation, both with 50,000 particles. Simulations with larger *dCylDp* required more time (e.g., about 12 hours for the shear cell with 400,000 particles).

ANN model development

	Bayesian	Gaussian	ANN
Coeff. of determination (R^2)	0.860	0.843	0.959
Root mean squared error	0.057	0.061	0.031
Mean absolute error	0.042	0.038	0.025
Mean squared error	0.003	0.004	0.001

Table 4: Regression methods quantitative comparison.

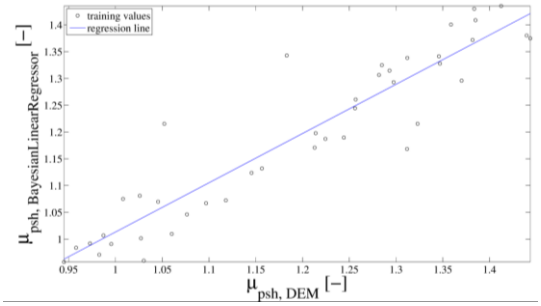

Figure 3: Regression line for the Bayesian linear prediction with the test samples.

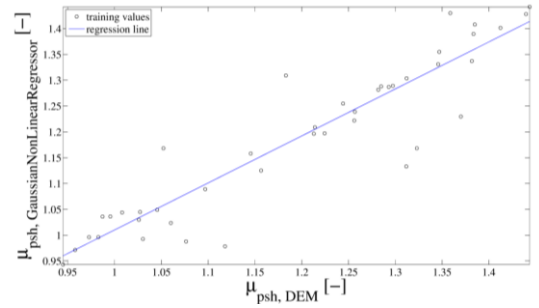

Figure 4: Regression line for the Gaussian nonlinear prediction with the test samples.

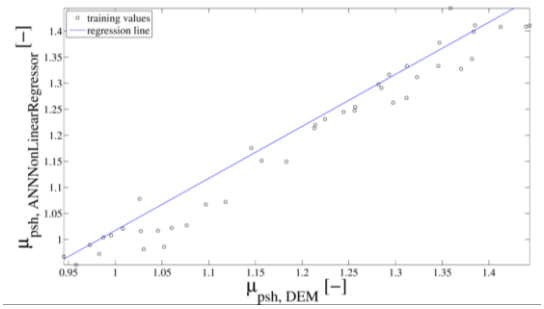

Figure 5: Regression line for the ANN with the test samples.

First, we determined the regressions of the bulk behaviour parameters, for instance the μ_{psh}, with a Bayesian linear prediction (Figure 3) and a Gaussian nonlinear prediction (Figure 4). Later we obtained Figure 5, where the corresponding plot for the *ANN* with the maximum R^2 is shown. Table 4 shows a quantitative comparison between the three methods. In fact, we achieved a $R^2 = 0.96$ for an *ANN* with fifteen neurons. Increasing the number of neurons did not improve the R^2; it even started to oscillate with higher numbers of neurons. We subsequently obtained the optimal number of neurons for all *ANNs*. Further, we processed the random combinations (Table 3) with the *ANN*. The *ANN* evaluation was significantly faster than the *DEM* simulations. The individuation of the numerical bulk behaviours for all the *DEM* combinations did not take more than a few seconds on a single core).

Experiments and Parameter Identification

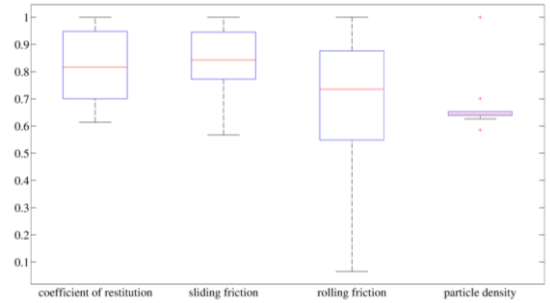

Figure 6: Box Plot, *SSC*, σ_n = 10,070 Pa, P. = 1.

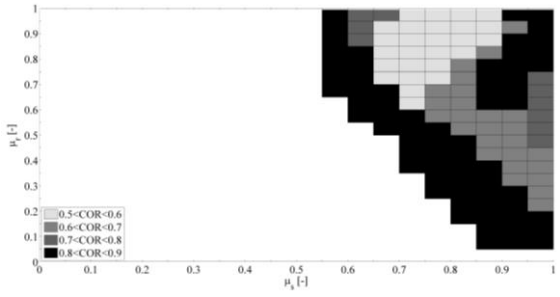

Figure 7: Density Plot, *SSC*, σ_n = 10,070 Pa, P. = 1.

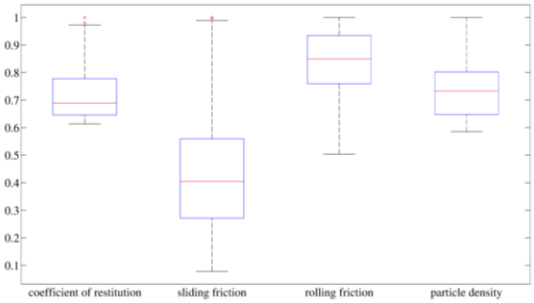

Figure 8: Box Plot, AoR.

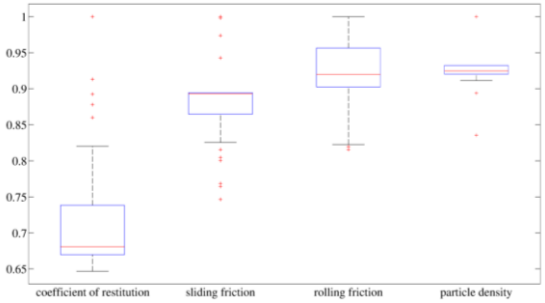

Figure 9: Box Plot, *SSC*, σ_n = 10,070 Pa, P. = 1. & AoR.

Experimental values identifying the bulk behavior, μ_{psh}, μ_{sh} and ρ_b, of sinter fine were acquired through *SSC* tests. The ρ_b has an average of 1,760 kg/m^3 with a 42 kg/m^3 deviation. Two *AoR* tests were performed that gave an average angle of 38.85°. We obtained the radius (R) mean and standard deviations, as shown in Table Table 1, from sieving experiments. The comparison between numerical and experimental behaviours led to a first series of marked combinations (*MC1*) for one load condition of the shear cell (σ_n =10,070 Pa, P=1.0), as plotted in Figure 6, with values normalized over the maximum values, shown in Table 5. Also the remaining box plots present normalized values. Both the ρ_p and the μ_s, however, show a narrow confidence interval, which demonstrates their influence and the ability of this procedure to find valid *DEM* parameters. These results agree with our examination of the ratio of the standard deviation to the range, see Table 5. Further, we observed that various *DEM* parameter combinations could reproduce the experimental behaviour, and thus evaluated their mutual dependencies. This is shown more clearly in a density plot (see Figure 7 for *MC1*) of the particles' coefficient of restitution (*COR*) in relation to the coefficients of sliding friction (μ_s) and rolling friction (μ_r); in the white area, no valid sets of simulation parameters can be found. In each cell the valid sets are grouped according to the 4 different COR ranges. Each cell is coloured according to the group with the most members. Multiple combinations (250,407 or 4% of the total) of μ_s and μ_r reproduced the experimental behaviour with varying *COR*. This underlines once more their correlation, as already stated by Wensrich and Katterfeld (2012).

We then processed the random combinations with the *AoR ANN*. In Figure 8 the box plot for the same criteria as before can be seen. In accordance with theory (Wensrich, Katterfeld 2012), in a simulation dominated by rolling particles, the coefficient of rolling friction has the maximum influence.

Finally, we extracted from the *MC1* values the *AoR ANN* behaviour and compared it with the experimental one. As can be seen in the box plot in Figure 9, the confidence interval is very small, indicating that all the parameters but the *COR* played an important role, and demonstrating the reliability of these parameter combinations in representing the bulk behaviour. From the initial 6,250,000 combinations, only 3,884 were valid (0.0621%), see Table 5.

	type	SSC	AoR	SSC & AoR
μ_s (-)	mean	0.831	0.177	0.664
	std. dev. (SD)	0.097	0.095	0.029
	max	0.864	0.8643	0. 745
	range (R)	0.9	0.9	0.9
	SD / R	0.108	0.106	0.032
μ_r (-)	mean	0.692	0.830	0.916
	std. dev. (SD)	0.215	0.193	0.042
	max	0.981	0.830	0.989
	range (R)	0.9	0.9	0.9
	SD / R	0.239	0.214	0.046
COR (-)	mean	0.708	0.590	0.590
	std. dev. (SD)	0.104	0.073	0.065
	max	0.989	0.989	0.820
	range (R)	0.4	0.4	0.4
	SD / R	0.259	0.183	0.161
ρ_p (kg/m^3)	mean	2245.7	3192.8	2283.9
	std. dev. (SD)	80.5	277.4	67.1
	max	3498.6	3498.6	2452.2
	range (R)	1500	1500	1500
	SD / R	0.054	0.185	0.045
valid comb'ns	number	290203	816552	3884
	(%)	4.64	13.06	0.06

Table 5: DEM valid values.

Macroscopic application

As explained in the Application section, we divided the first of the boxes filled by the chute in three layers with the same dimensions, from 6 on top to 8 on bottom, see Figure 10. The volume over these layers was not considered, because it was continuously supplied of particles from the chute. In Figure 11 the percentage of the total volume of the particles available in each layer at steady-state, grouped by radius, is shown. We could clearly see how the larger particles disposed mostly in the bottom layer, validating the realized design.

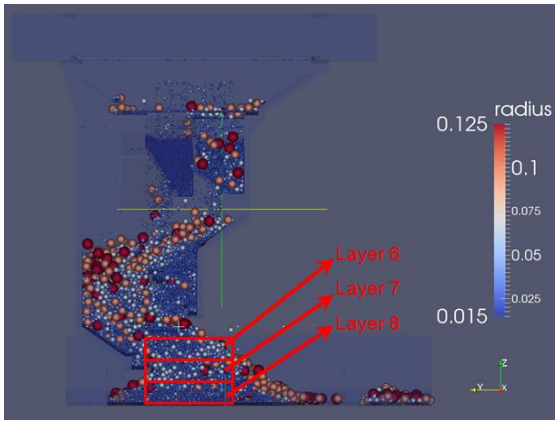

Figure 10: DEM simulation layout.

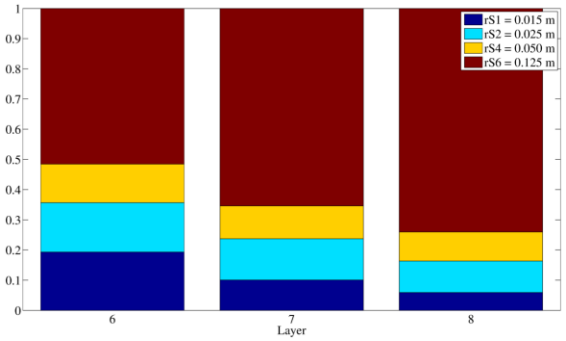

Figure 11: DEM segregation of particles in the chute.

CONCLUSION

We have presented a two-step method for *DEM* simulation parameter identification. In the first step, an artificial neural network is trained using dedicated *DEM* simulations in order to predict bulk behaviours as function of a set of *DEM* simulation parameters. In the second step, this artificial neural network is then used to predict the bulk behaviour of a huge number of additional *DEM* parameter sets. The main findings of this study can be summarized as follows:

- An artificial neural network can be trained by a limited number of dedicated *DEM* simulations. The trained artificial neural network is then able to predict granular bulk behaviour.
- The correctness of the training can be established through standard statistical methods.
- This prediction of granular bulk behaviour is much more efficient than computationally expensive *DEM* simulations. Thus, the macroscopic output associated with a huge number of parameter sets can be studied.
- If the predictions of the artificial neural network are compared to a bulk experiment, valid sets of *DEM* simulation parameters can be readily deduced for a specific granular material.
- This *DEM* parameter identification method can be applied to arbitrary bulk experiments. Combining two artificial neural networks which predict two different bulk behaviours leads to winnowing the set of valid *DEM* simulation parameters.
- The parameters collected with this method can be trustworthy used for large scale simulations.

As part of future work, we will develop this method further by considering different fractions of granular materials, which will lead to size-dependent sets of *DEM* simulation parameters.

AKNOWLEDGEMENTS

This study was funded by Christian Doppler Forschungsgesellschaft, Siemens VAI Metals Technologies and Voestalpine Stahl. The authors gratefully acknowledge their support.

REFERENCES

AI, J., CHEN, J., ROTTER, J.M. and OOI, J.Y., 2011. Assessment of rolling resistance models in discrete element simulations. *Powder Technology*, **206**(3), pp. 269-282.

AIGNER, A., SCHNEIDERBAUER, S., KLOSS, C. and PIRKER, S., 2013. Determining the coefficient of friction by shear tester simulation. *3rd International Conference on Particle-Based Methods*, , pp. 335-342.

ALENZI, A., MARINACK, M., HIGGS, C.F. and MCCARTHY, J.J., 2013. DEM validation using an annular shear cell. *Powder Technology*, **248**(0), pp. 131-142.

BENVENUTI, L., AIGNER, A., QUETESCHINER, D., COMBARROS, M., PIRKER, S. and KLOSS, C., 2014. Establishing the predictive capabilities of DEM simulations: sliding and rolling friction coefficients of non-spherical particles, *CFD 2014 Proceedings*, June 2014.

BENVENUTI, L., KLOSS, C. and PIRKER, S., *Identification of DEM Simulation Parameters by Artificial Neural Networks and Bulk Experiments.*

CLEARY, P.W. and SAWLEY, M.L., 2002. DEM modelling of industrial granular flows: 3D case studies and the effect of particle shape on hopper discharge. *Applied Mathematical Modelling*, **26**(2), pp. 89-111.

COMBARROS, M., FEISE, H.J., ZETZENER, H. and KWADE, A., 2014. Segregation of particulate solids: Experiments and DEM simulations. *Particuology*, **12**(0), pp. 25-32.

CUNDALL, P.A. and STRACK, O.D.L., 1979. A discrete numerical model for granular assemblies. *Geotechnique*, **29**(Volume 29, Issue 1), pp. 47-65(18).

DI RENZO, A. and DI MAIO, F.P., 2004. Comparison of contactforce models for the simulation of collisions in DEMbased granular flow codes. *Chemical Engineering Science*, **59**(3), pp. 525-541.

HAYKIN, S., 2009. *Neural Networks and Learning Machines.* Prentice Hall.

KLOSS, C., GONIVA, C., HAGER, A., AMBERGER, S. and PIRKER, S., 2012. Models, algorithms and validation for opensource DEM and CFDDEM. *Progress in Computational Fluid Dynamics, an International Journal*, **12**(2), pp. 140-152.

OBERKAMPF, W.L. and ROY, C.J., 2010. *Verification and Validation in Scientific Computing.* Cambridge University Press.

TSAFNAT, N., AMANAT, N. and JONES, A.S., 2011. Analysis of coke under compressive loading: A combined approach using microcomputed tomography, finite element analysis, and empirical models of porous structures. *Fuel*, **90**(1), pp. 384-388.

VAFERI, B., SAMIMI, F., PAKGOHAR, E. and MOWLA, D., 2014. Artificial neural network approach for prediction of thermal behavior of nanofluids flowing through circular tubes. *Powder Technology*, **267**(0), pp. 1-10.

VU-QUOC, L. and ZHANG, X., 1999. An accurate and efficient tangential force-displacement model for elastic frictional contact in particle-flow simulations. *Mechanics of Materials*, **31**(4), pp. 235-269.

WENSRICH, C.M. and KATTERFELD, A., 2012. Rolling friction as a technique for modelling particle shape in DEM. *Powder Technology*, **217**(0), pp. 409-417.

